.

Mechanical, electronic and catalytic properties of 2H–1T^0 MoS_2 heterointerfaces†

Xiangru Huang,[ab] Yuan Chang,[a] Shi Qiu,[a] Hongsheng Liu, [a] Vitali Shymanski[b] and Junfeng Gao *[ab]

Using first-principles calculations, we comprehensively explored the influence of 2H–1T^0 heterointer-faces in molybdenum disulfide (MoS_2) on the mechanical, electronic and catalytic properties of MoS_2. The S-orientated interfaces, including interfaces with interstitial S or S vacancies, were adopted as sam-ples. All the heterostructures show a smaller yield stress than 2H and 1T^0 MoS_2, and fractures always occur at the interface. The heterostructures are either metallic or half-metallic. Some of the heterointer-faces show great catalytic ability for the hydrogen evolution reaction (HER). In particular, the Gibbs free energy of H adsorption is as low as 0.028 eV for the S-LU-sint structure. Moreover, a small strain of 4% can improve the HER catalytic activity for several heterostructures. Our results show that 2H–1T^0 MoS_2 heterointerfaces are potential catalysts for the HER.

1. Introduction

The successful fabrication of graphene in 2004 using the mechan-ical cleavage method[1] introduced research into two-dimensional materials (2D). In recent years, two-dimensional materials have been greatly developed with lots of 2D materials being obtained or predicted.[2–6] Compared with bulk materials, 2D materials are unique with unprecedented physical and chemical properties due to the quantum confinement effect.[2–8] 2D materials naturally have large surface areas[9] and are ideal catalytic templates.[10] Among the 2D materials, molybdenum sulfide (MoS_2) has been widely studied and shows potential applications in electronic and optoelectronic devices.[11] For 2D MoS_2, it has two polytypic struc-tures, which include 2H-MoS_2 (trigonal prismatic coordination) and 1T-MoS_2 (octahedral symmetry). The 2H-to-1T phase transi-tion can be triggered by chemical exfoliation[12] or via the electro-chemical incorporation of S vacancies.[13] Actually, 1T–2H interfaces are unstable and a distortion will occur, transforming them to 1T^0–2H interfaces.[14]

Compared with intrinsic 2D materials, boundaries, defects and interfaces could lead to discontinuous structures and charge redistribution,[15] which will introduce new properties. Previous studies have shown that doping, defect engineering, facet engineering, phase regulation, and interface engineering can enhance the HER activity of MoS_2.[16–23] MoS_2–$MoSe_2$ lateral heterojunctions can minimize the lattice thermal conductivity.[24,25] Due to their similar lattice constants, a perfect intralayer hetero-structure can be constructed by connecting 2H-MoS_2 and 1T^0-MoS_2. A clear intralayer 1T^0/2H MoS_2 interface has been obtained in experiments by intercalating Li atoms in 2H-MoS_2.[26] Recently, using density functional theory (DFT) calculations, Zou and co-workers explored the detailed atomic structures and migra-tion processes of 2H/1T^0 MoS_2 intralayer heterointerfaces.[14] They showed that armchair interfacial heterointerfaces were not stable and that stable structures formed for either Mo- or S-orientated zigzag interfaces. Intralayer heterostructures may introduce inter-esting properties and play an important role in their applications. Therefore, investigation of the physical and chemical properties of 2H/1T^0 MoS_2 intralayer heterostructures with zigzag interfaces is an interesting issue. However, until now, there is a lack of research on this topic.

Here, using DFT calculations, the mechanical, electronic and catalytic properties of 2H–1T^0 intralayer heterostructures of MoS_2 with zigzag interfaces were systematically explored. The interfaces weaken the mechanical strength but greatly improve the HER catalytic performance compared with pristine MoS_2 in either the 2H phase or the 1T^0 phase. For some heterostruc-tures, a small tensile strain can improve the HER catalytic activity.

2. Computational methods

Our DFT calculations were performed using the Vienna ab initio simulation package (VASP)[27–29] based on plane wave basis sets.

[a] Key Laboratory of Materials Modification by Laser, Ion and Electron Beams (Dalian University of Technology), Ministry of Education, Dalian, 116024, China.
E-mail: gaojf@dlut.edu.cn
[b] Dalian University of Technology and Belarusian State University Joint Institute & Innovation Center, China

The projector-augmented wave (PAW)[30,31] potentials were adopted to describe the electron–ion interactions. According to previous studies,[32,33] the Perdew–Burke–Ernzerhof (PBE) functional underestimates the band gap of MoS_2 by about 23% compared with DFT+U and hybrid HSE06 methods, but the main character of the bands agrees well with that calculated using DFT+U and hybrid HSE06 methods. Therefore, reason-able results for the catalytic performance of MoS_2 heterostruc-tures can be obtained using the PBE functional. Considering the computing costs, we used standard DFT instead of DFT+U and hybrid HSE06 methods. All structures are fully relaxed. A convergence criterion of 10^{-5} eV for the total energies and a convergence criterion of 0.02 eV $Å^{-1}$ for force were used.

$1 \times 8 \times 1$ Monkhorst–Pack grids are used for 2H–1T^0 hetero-structures during the structural relaxation. The kinetic energy cutoff was set to 400 eV. The vacuum-layer thickness is larger than 10 Å.

The intralayer heterostructures are based on 1T^0-MoS_2 and 2H-MoS_2, because the 1T phase is metastable and converts into the 1T^0 phase with lower symmetry.[14,34] The 1T^0 phase can be viewed as a distorted 1T phase and it has distorted Mo–Mo bonds (two Mo–Mo bonds with different lengths, where one is named the short unit (SU) with short Mo–Mo bonds, and the other is the long unit (LU) with a significantly larger Mo–Mo distance[14]). For single-layer 1T^0-MoS_2, Mo atoms are sand-wiched between two layers of S atoms. The difference between the 1T^0 phase and the 2H phase is the way that six S atoms connect to the same Mo atom.[35–37] The 2H/1T^0 MoS_2 intralayer heterostructures are constructed by connecting a series of rectangular supercells of 1T^0-MoS_2 (2×1) and 2H-MoS_2 (2×3 and 2×4).

3. Results and discussion

Firstly, we constructed a series of 2H–1T^0 MoS_2 intralayer heterostructures with zigzag interfaces, including the struc-tures with interstitial S or S vacancies on either the 2H- or 1T^0-MoS_2 side. Considering the orientation, interstitial S, S vacancies and the relative length of the Mo–Mo bonds, there are 16 kinds of 2H–1T^0 heterointerface.[14] However, only 7 of them are stable after geometry optimization. The seven struc-tures are named as follows: S-LU-0 (interface with relatively long Mo–Mo bonds), S-LU-1T^0 (S vacancies on the 1T^0 side of the S-LU-0 interface), S-LU-2H (S vacancies on the 2H side of the S-LU-0 interface), S-LU-sint (interstitial S on the 2H side of the S-LU-0 interface), S-SU-0 (interface with relatively short Mo–Mo bonds), S-SU-1T^0 (S vacancies on the 1T^0 side of the S-SU-0 interface), and S-SU-2H (S vacancies on the 2H side of the S-SU-0 interface). The optimized structures of the seven heterostruc-tures are shown in Fig. 1.

In order to estimate the stability of the seven 2H–1T^0 heterostructures, the formation energies are calculated as follows:

$$E_{f1} = \frac{1}{L}\left(E_{total} - N_1 E_{1T^0} - N_2 E_{2H}\right) \quad (1)$$

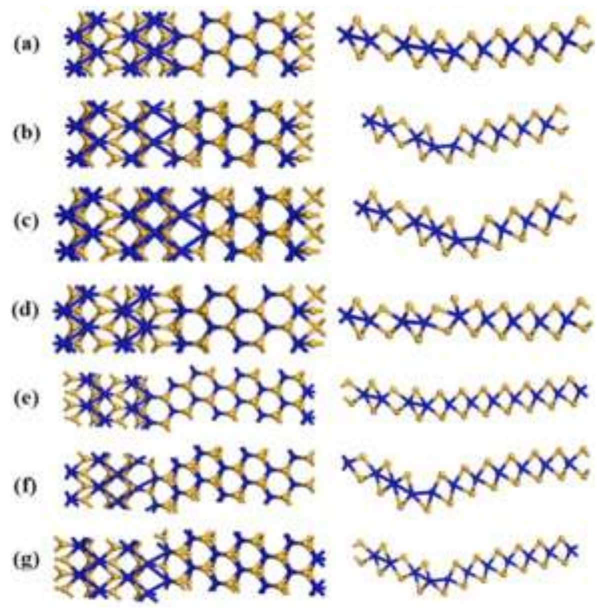

Fig. 1 Top view (left) and side view (right) of the seven stable 2H–1T^0 MoS_2 intralayer heterostructures with zigzag interfaces: (a) S-LU-0, (b) S-LU-1T^0, (c) S-LU-2H, (d) S-LU-sint, (e) S-SU-0, (f) S-SU-1T^0, and (g) S-SU-2H. Blue and yellow spheres represent Mo and S atoms, respectively.

$$E_{f2} = \frac{1}{L}\left(E_{total} - N_1 E_{1T^0} - N_2 E_{2H} + E_S\right) \quad (2)$$

$$E_{f3} = \frac{1}{L}\left(E_{total} - N_1 E_{1T^0} - N_2 E_{2H} - E_S\right) \quad (3)$$

Here, E_{f1} is the formation energy of the heterostructure without any defects, E_{f2} is the formation energy of the hetero-structure with S vacancies, and E_{f3} is the formation energy of the heterostructure with interstitial S. E_{total} is the total energy of the heterostructure, E_{1T^0} is the total energy of the unit cell of the 1T^0 phase, and E_{2H} is the total energy of the unit cell of the 2H phase; N_1 is the number of rectangular unit cells of the 1T^0 phase in the heterostructure, and N_2 is the number of rectan-gular unit cells of the 2H phase in the heterostructure; E_S is the total energy of the S atoms, and L is the length of the interface. The formation energies of these stable structures are listed in Table 1. According to the formation energy, for the S-LU-interfaces: S-LU-0 is the most stable one with the formation energy of 1.053 eV $Å^{-1}$; and for S-SU-interfaces: S-SU-0 is the

Table 1 Formation energies of the seven stable 2H–1T^0 structures

Name	N_1	N_2	E_{total} (eV)	$E_{formation}$ (eV $Å^{-1}$)
S-LU-0	2	3	200.35	1.053
S-LU-1T^0	2	3	194.17	1.191
S-LU-2H	2	3	193.66	1.227
S-LU-sint	2	3	204.45	1.014
S-SU-0	2	4	246.57	0.832
S-SU-1T^0	2	4	240.32	0.958
S-SU-2H	2	4	239.76	0.997

most stable one with the formation energy of 0.832 eV Å ^{1}. Our results agree with those of Zou et al.[14]

3.1 Mechanical properties of 2H–$1T^{0}$ heterointerfaces in MoS_2

To investigate the effect of the heterointerfaces on the mechan-ical properties of the MoS_2 monolayer, gradually increasing the tensile strain perpendicular to the interface was applied for all seven 2H–$1T^{0}$ heterostructures.[37] The stress calculated using VASP (s_0) should be modified to the actual stress (s) using

$$s = \frac{c}{d} s_0 \tag{4}$$

Here, c is the lattice constant perpendicular to the monolayer, and d is the thickness of the heterostructure, which is defined as the distance between the highest and lowest S atoms.

According to eqn (4), we plot the stress–strain curves for all seven heterostructures, as shown in Fig. 2. For $1T^{0}$ MoS_2, when the strain reaches 12%, the stress suddenly falls, resulting in a yield stress of 24.30 GPa. By contrast, for 2H MoS_2, when the yield strain reaches 24% the yield stress is as high as 54.07 GPa. Therefore, the 2H phase is more robust than the $1T^{0}$ phase against stress. For the 2H–$1T^{0}$ heterostructures, similar stress– strain curves are found but with different yield stresses. To directly show the effect of the heterointerface on the mechan-ical properties of MoS_2, the yield stress for $1T^{0}$ MoS_2, 2H MoS_2

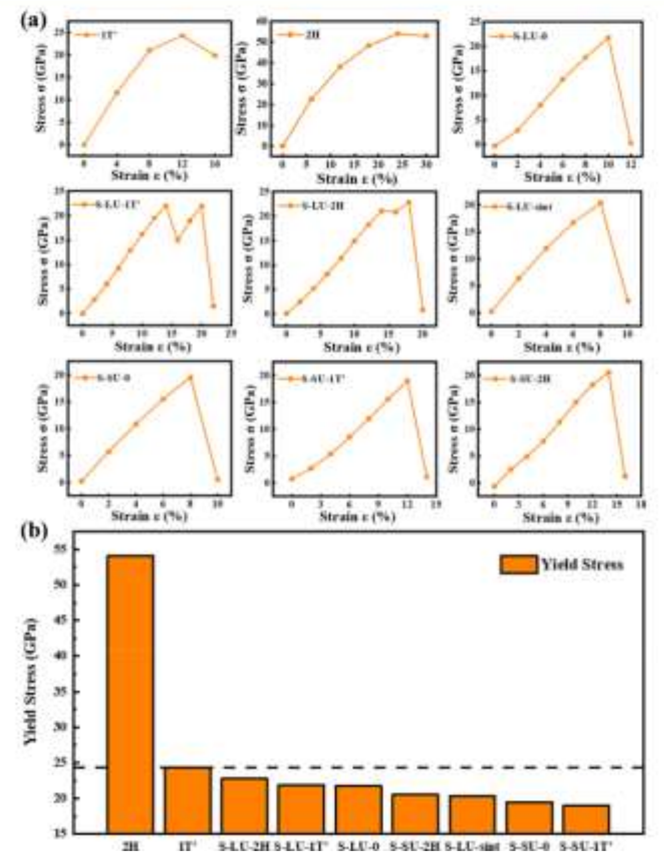

Fig. 2 (a) Strain–stress curves and (b) yield stress for $1T^{0}$ MoS_2, 2H MoS_2 and the $1T^{0}$–2H heterostructures.

and the $1T^{0}$–2H heterostructures are compared in Fig. 2b. The yield stress for all the heterostructures is lower than that of the $1T^{0}$ and 2H phases. Therefore, the interface weakens the yield strength. Among the seven heterostructures, S-SU-$1T^{0}$ has the lowest yield stress and S-LU-2H has the highest yield stress. By checking the atomic structures after yield strain, we find that the fracture always starts from the interface. Therefore, under strain, stress will mainly accumulate at the interface.

3.2 Electronic properties of 2H–$1T^{0}$ heterointerfaces in MoS_2

Firstly, we calculated the electronic band structures of the perfect $1T^{0}$ phase and the 2H phase for the MoS_2 monolayer, which are shown in Fig. S1 in the ESI.† The band structure shows that 2H-MoS_2 is a semiconductor with a band gap of 1.773 eV (Fig. S1a, ESI†). By contrast, $1T^{0}$-MoS_2 is metallic (Fig. S1b, ESI†). This in in accordance with previous results.[38,39] Then, the electronic band structures of all the $1T^{0}$–2H hetero-structures considered here are calculated and are shown in Fig. 3. S-LU-0, S-LU-$1T^{0}$, S-LU-2H, S-LU-sint and S-SU-$1T^{0}$ are all metallic; S-SU-0 and S-SU-2H are half-metallic. Therefore, in the hetero-structures, due to the presence of the $1T^{0}$ phase and the interface, the semiconductor character of the 2H phase is overridden. Neither interstitial S nor S vacancies at the interface can change the metallicity.

Applying tensile stress to a two-dimensional material may produce a phase change and may change the band gap.[40] To investigate the strain effect on the electronic properties, band structures of all the $1T^{0}$–2H heterostructures under different strains were calculated and are shown in Fig. 3. For metallic heterostructures, including S-LU-0, S-LU-$1T^{0}$, S-LU-2H, S-LU-sint and S-SU-$1T^{0}$, strain does not change the metallic character

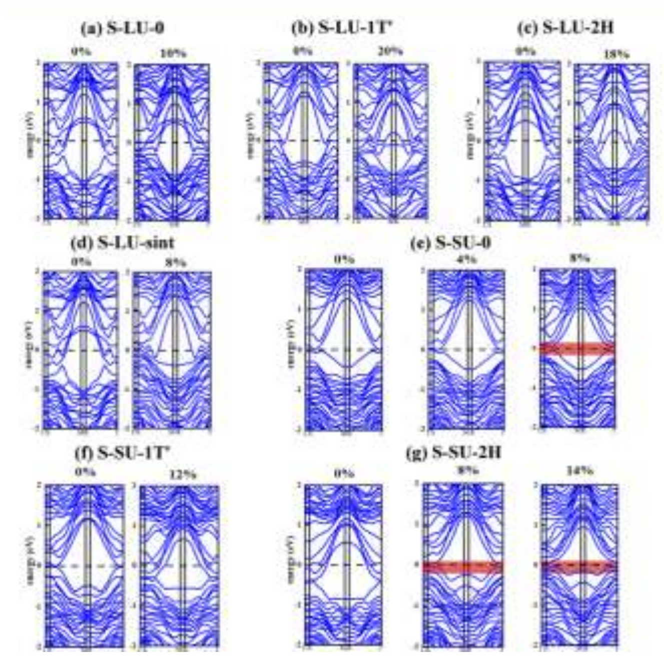

Fig. 3 Electronic band structures of the different $1T^{0}$–2H MoS_2 hetero-structures under different strains.

but changes the bands crossing the Fermi level. By contrast, a small band gap can be opened under a strain of 8% for S-SU-0 and of both 8% and 14% for the S-SU-2H heterostructure.

3.3 Catalytic properties of 2H–$1T^0$ MoS_2 heterostructures

The hydrogen evolution reaction (HER) is an important electro-catalytic reaction that occurs in hydrogen fuel cells and water electrolysers. MoS_2, instead of precious metals, is a new catalyst for the HER. Very recent studies have demonstrated that monolayer MoS_2 nanosheets with the 1T metallic phase synthe-sized via chemical exfoliation exhibited a superior HER cataly-tic activity to those with the 2H semiconducting phase.[41]

Here we explore the HER catalytic activity of the 2H–$1T^0$ MoS_2 heterointerfaces. One H atom is put above the interface. As a comparison, we also explore the catalytic activity of perfect monolayer MoS_2 in both the $1T^0$ and 2H phases. The optimized structures for the H adatoms on these monolayers are shown in Fig. 4. For $1T^0$ and 2H MoS_2, the H atom prefers to adsorb on the S atom. By contrast, the H atom prefers to adsorb on the Mo atom for all interfaces except for S-LU-sint. For S-LU-sint, the H atom prefers to adsorb on the interstitial S atom.

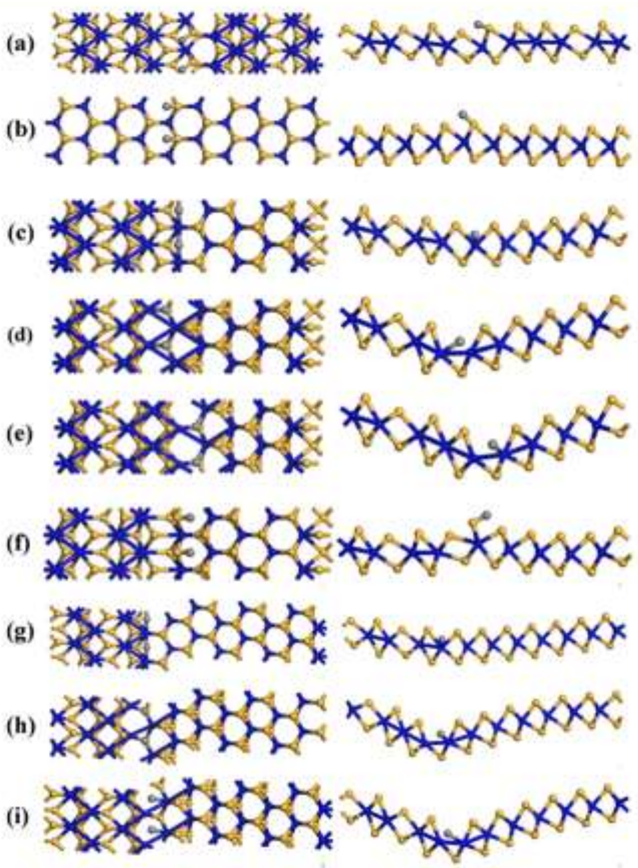

Fig. 4 Top view (left) and side view (right) of the optimized structures for H adatoms adsorbed on MoS_2 monolayers: (a) $1T^0$, (b) 2H, (c) S-LU-0, (d) S-LU-$1T^0$, (e) S-LU-2H, (f) S-LU-sint, (g) S-SU-0, (h) S-SU-$1T^0$, and (i) S-SU-2H. Blue spheres denote Mo atoms, yellow spheres denote S atoms, and grey spheres denote H atoms.

Table 2 Gibbs free-energy of these perfect structures

Name	DE_H (eV)	Charge gained/ donated	$DE_{zero\text{-}point}$ (eV)	TDS (eV)	DG (eV)
$1T^0$	1.486	0.137	0.224	0.0082	1.701
2H	1.370	0.0127	0.233	0.0061	1.596
S-LU-0	0.344	0.1957	0.230	0.0022	0.572
S-LU-$1T^0$	0.631	0.3083	0.180	0.0073	0.458
S-LU-2H	0.450	0.2957	0.197	0.0044	0.258
S-LU-sint	0.271	0.0424	0.249	0.0057	0.028
S-SU-0	0.299	0.2016	0.220	0.0043	0.515
S-SU-$1T^0$	0.493	0.2985	0.197	0.0035	0.299
S-SU-2H	0.732	0.3382	0.241	0.0019	0.493

We use the Gibbs free-energy of the adsorption of an atomic hydrogen DG as a most important criterion for measuring the HER activity.[13,42,43] The stability of hydrogen adsorption is described using the hydrogen chemisorption energy DE_H, which is calculated as:

$$DE_H = E_1 - E_2 - \frac{1}{2}E_{H_2} \quad (5)$$

Here, E_1 is the total energy of the 2H–$1T^0$ MoS_2 heterointer-faces with one hydrogen, E_2 is the total energy of the 2H–$1T^0$ MoS_2 heterointerfaces, and E_{H_2} is the total energy of a hydrogen molecule in the gas phase. So, we can obtain the formula for the Gibbs free-energy DG:

$$DG = DE_H + DE_{zero\text{-}point} \quad TDS. \quad (6)$$

Here, $DE_{zero\text{-}point}$ is the zero-point energy, and TDS is the entropy term.

According to the hydrogen chemisorption energy DE_H listed in Table 2, the H atom strongly binds with the S-LU-$1T^0$ and S-SU-2H interfaces. By contrast, a moderate interaction between the H atom and the interface can be obtained for the S-LU-sint interface. Bader charge analysis[44] was performed to quantify the amount of charge gained/donated by the adsorbing H atom, as shown in Table 2. The stronger the binding the larger the charge transfer. For an H atom adsorbed on the S-LU-sint interface, the H atom donates electrons to the heterostructure because the H atom binds with an S atom. For the H atom adsorbed on other interfaces, the H atom gains electrons from the heterostructure because the H atom binds with a Mo atom.

The Gibbs free-energy values for the adsorption of atomic hydrogen on different monolayers are listed in Table 2 and Fig. 5a. In general, the formation of the interface significantly enhances the HER activity. According to previous studies, |DG| r 0.3 eV shows that the structure has good catalytic activity. Therefore, structures with good catalytic effects are S-LU-2H (DG = 0.258 eV), S-LU-sint (DG = 0.028 eV) and S-SU-$1T^0$ (DG = 0.299 eV). We can also see that the Gibbs free-energy of the interface with interstitial S and S vacancies is lower than the Gibbs free-energy of the '0' structure. That means inter-stitial S and S vacancies can further enhance the HER activity.

To check the lateral domain size effect on the HER activity, an S-LU-sint heterostructure with the domain size for both the 2H and $1T^0$ phases twice the size as that shown in Fig. 4f was

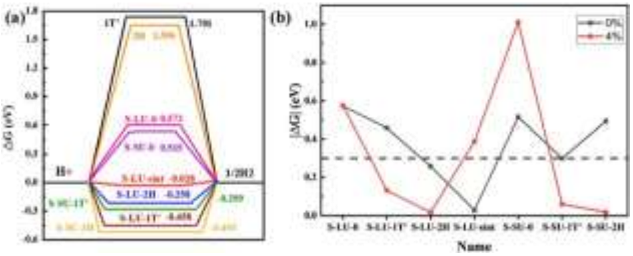

Fig. 5 (a) Gibbs free-energy during the HER for different interface configurations. (b) Gibbs free energy after applying 4% tensile stress to the different interface configurations.

constructed (shown in Fig. S2, ESI†). The Gibbs free-energy for H adsorption was calculated to be 0.040 eV, which is only 12 meV smaller than the original S-LU-sint heterostructure (0.028 eV). Therefore, the lateral size of the 2H or $1T^0$ MoS_2 domain has little effect on the HER activity. Moreover, different adsorption sites for H adsorption were tested. The H adsorp-tion energy and the Gibbs free-energy of adsorption for the H atom adsorbed on different sites of the S-LU-sint heterostruc-ture are shown in Table S1 (ESI†), which shows that the inter-face site is the most stable adsorption site and exhibits the best catalytic performance.

Meanwhile, mechanistic factors were considered for this hydrocatalytic process. Under 4% tensile stress, the catalytic activity of S-LU-$1T^0$ (DG = 0.131 eV), S-LU-2H (DG = 0.016 eV), S-SU-$1T^0$ (DG = 0.059 eV), and S-SU-2H (DG = 0.017 eV) can be improved, as shown in Fig. 5b. However, the catalytic activity of S-LU-sint and S-SU-0 are weakened under strain. Because the tensile strain will weaken the chemical bonds at the interface, defects, such as S vacancies, are expected to be easier to arise. Therefore, to a certain degree, mechanical strain can poten-tially induce the formation of defects.

4. Conclusions

In conclusion, we systematically investigated the stability of $1T^0$/2H MoS_2 intralayer heterostructures. S-LU-0 and S-SU-0 are more stable than interfaces with interstitial S or S vacancies. The mechanical, electronic and catalytic properties as well as the strain effects were also studied. The interfaces weaken the mechanical strength because the stress will be focused at the interface under stain. All the stable heterointerfaces show metallic or semi-metallic properties. A small tensile strain can effectively change the electro-nic properties of the heterostructures. In particular, for the S-SU-0 and S-SU-2H heterostructures, a small band gap can be opened under a strain of 8%. The heterointerfaces in MoS_2 can greatly enhance the HER activity. Moreover, strain can also improve the HER activity for the S-LU-$1T^0$, S-LU-2H, S-SU-$1T^0$ and S-SU-2H interfaces. Our results show that $1T^0$/2H MoS_2 intralayer hetero-structures are potential HER catalysts.

Conflicts of interest

There are no conflicts to declare.

Acknowledgements

This work was supported by the National Natural Science Foundation of China (Grant No. 12074053, 91961204, 12004064), the Fundamental Research Funds for the Central Universities (DUT21LAB112, DUT22ZD103), the Research Fund for International Cooperation of DUT-BSU Joint Institute (ICR2106), and 2022 National Foreign Expert Project (G2022127004L) and XingLiaoYingCai Project of Liaoning province, China (XLYC1907163). The authors also acknowledge computing supercomputer of Tianjin center and Hongzhiwei Technology.

References

1 K. S. Novoselov, A. K. Geim, S. V. Morozov, D. Jiang, Y. Zhang, S. V. Dubonos, I. V. Grigorieva and A. A. Firsov, Electric Field Effect in Atomically Thin Carbon Films, Science, 2004, 306, 666–669.

2 K. S. Novoselov, D. Jiang, F. Schedin, T. J. Booth, V. V. Khotkevich, S. V. Morozov and A. K. Geim, Two-dimensional atomic crystals, Proc. Natl. Acad. Sci. U. S. A., 2005, 102, 10451–10453.

3 S. Z. Butler, S. M. Hollen, L. Y. Cao, Y. Cui, J. A. Gupta, H. R. Gutie´rrez, T. F. Heinz, S. S. Hong, J. X. Huang, A. F. Ismach, E. Johnston-Halperin, M. Kuno, V. V. Plashnitsa, R. D. Robinson, R. S. Ruoff, S. Salahuddin, J. Shan, L. Shi, M. G. Spencer, M. Terrones, W. Windl and J. E. Goldberger, Progress, Challenges, and Opportunities in Two-Dimensional Materials Beyond Graphene, ACS Nano, 2013, 7, 2898–2926.

4 C. L. Tan, X. H. Cao, X.-J. Wu, Q. Y. He, J. Yang, X. Zhang, J. Z. Chen, W. Zhao, S. K. Han, G.-H. Nam, M. Sindoro and H. Zhang, Recent Advances in Ultrathin Two-Dimensional Nanomaterials, Chem. Rev., 2017, 117, 6225–6331.

5 M. Chhowalla, H. S. Shin, G. Eda, L.-J. Li, K. P. Loh and H. Zhang, The chemistry of two-dimensional layered transi-tion metal dichalcogenide nanosheets, Nat. Chem., 2013, 5, 263–275.

6 G. R. Bhimanapati, Z. Lin, V. Meunier, Y. Jung, J. Cha, S. Das, D. Xiao, Y. Son, M. S. Strano, V. R. Cooper, L. B. Liang, S. G. Louie, E. Ringe, W. Zhou, S. S. Kim, R. R. Naik, B. G. Sumpter, H. Terrones, F. N. Xia, Y. L. Wang, J. Zhu, D. Akinwande, N. Alem, J. A. Schuller, R. E. Schaak, M. Terrones and J. A. Robinson, Recent Advances in Two-Dimensional Materials beyond Graphene, ACS Nano, 2015, 9, 11509–11539.

7 K. S. Novoselov, A. K. Geim, S. V. Morozov, D. Jiang, M. I. Katsnelson, I. V. Grigorieva, S. V. Dubonos and A. A. Firsov, Two-Dimensional Gas of Massless Dirac Fermions in Graphene, Nature, 2005, 438, 197–200.

8 Y. B. Zhang, Y.-W. Tan, H. L. Stormer and P. Kim, Experi-mental Observation of the Quantum Hall Effect and Berry's Phase in Graphene, Nature, 2005, 438, 201–204.

9 Y. Huang, J. J. Liang and Y. S. Chen, An Overview of the Applications of Graphene-Based Materials in Supercapaci-tors, Small, 2012, 8, 1805–1834.

10 D. H. Deng, K. S. Novoselov, Q. Fu, N. F. Zheng, Z. Q. Tian and X. H. Bao, Catalysis with two-dimensional materials

and their heterostructures, Nat. Nanotechnol., 2016, 11, 218–230.

11 Q. H. Wang, K. Kalantar-Zadeh, A. Kis, J. N. Coleman and M. S. Strano, Electronics and optoelectronics of two-dimensional transition metal dichalcogenides, Nat. Nano-technol., 2012, 7, 699–712.

12 A. Ambrosi, Z. Sofer and M. Pumera, 2H - 1T phase transition and hydrogen evolution activity of MoS2, MoSe2, WS2 and WSe2 strongly depends on the MX2 composition, Chem. Commun., 2015, 51, 8450–8453.

13 X. R. Gan, L. Y. S. Lee, K.-Y. Wong, T. W. Lo, K. H. Ho, D. Y. Lei and H. M. Zhao, 2H/1T Phase Transition of Multilayer MoS_2 by Electrochemical Incorporation of S Vacancies, ACS Appl. Energy Mater., 2018, 1, 4754–4765.

14 X. L. Zou, Z. H. Zhang, X. B. Chen and B. I. Yakobson, Structure and Dynamics of the Electronic Heterointerfaces in MoS_2 by First-Principles Simulations, J. Phys. Chem. Lett., 2020, 11, 1644–1649.

15 Z. H. Hu, Z. T. Wu, C. Han, J. He, Z. H. Ni and W. Chen, Two-dimensional transition metal dichalcogenides: interface and defect engineering, Chem. Soc. Rev., 2018, 47, 3100–3128.

16 J. F. Xie, J. D. Qi, F. C. Lei and Y. Xie, Modulation of electronic structures in two-dimensional electrocatalysts for the hydrogen evolution reaction, Chem. Commun., 2020, 56, 11910–11930.

17 J. F. Xie, X. Y. Yang and Y. Xie, Defect engineering in two-dimensional electrocatalysts for hydrogen evolution, Nano-scale, 2020, 12, 4283–4294.

18 J. F. Xie, L. Gao, H. L. Jiang, X. D. Zhang, F. C. Lei, P. Hao, B. Tang and Y. Xie, Platinum Nanocrystals Decorated on Defect-Rich MoS_2 Nanosheets for pH-Universal Hydrogen Evolution Reaction, Cryst. Growth Des., 2019, 19, 60–65.

19 J. F. Xie, H. C. Qu, J. P. Xin, X. X. Zhang, G. W. Cui, X. D. Zhang, J. Bao, B. Tang and Y. Xie, Defect-rich MoS_2 nanowall catalyst for efficient hydrogen evolution reaction, Nano Res., 2017, 10, 1178–1188.

20 J. F. Xie, J. P. Xin, G. W. Cui, X. X. Zhang, L. J. Zhou, Y. L. Wang, W. W. Liu, C. H. Wang, M. Ning, X. Y. Xia, Y. Q. Zhao and B. Tang, Vertically aligned oxygen-doped molybdenum disulfide nanosheets grown on carbon cloth realizing robust hydrogen evolution reaction, Inorg. Chem. Front., 2016, 3, 1160–1166.

21 J. F. Xie and Y. Xie, Structural Engineering of Electrocata-lysts for the Hydrogen Evolution Reaction: Order or Dis-order?, ChemCatChem, 2015, 7, 2568–2580.

22 J. F. Xie, J. J. Zhang, S. Li, F. Grote, X. D. Zhang, H. Zhang, R. X. Wang, Y. Lei, B. C. Pan and Y. Xie, Controllable Disorder Engineering in Oxygen-Incorporated MoS_2 Ultra-thin Nanosheets for Efficient Hydrogen Evolution, J. Am. Chem. Soc., 2013, 135, 17881–17888.

23 J. F. Xie, H. Zhang, S. Li, R. X. Wang, X. Sun, M. Zhou, J. F. Zhou, X. W. Lou and Y. Xie, Defect-Rich MoS_2 Ultrathin Nanosheets with Additional Active Edge Sites for Enhanced Electrocatalytic Hydrogen Evolution, Adv. Mater., 2013, 25, 5807–5813.

24 X. D. Duan, C. Wang, J. C. Shaw, R. Cheng, Y. Chen, H. L. Li, X. P. Wu, Y. Tang, Q. L. Zhang, A. L. Pan, J. H. Jiang, R. Q. Yu, Y. Huang and X. F. Duan, Lateral epitaxial growth of two-dimensional layered semiconductor heterojunctions, Nat. Nanotechnol., 2014, 9, 1024–1030.

25 G. Q. Ding, J. J. He, G. Y. Gao and K. L. Yao, Two-dimensional MoS_2-$MoSe_2$ lateral superlattice with mini-mized lattice thermal conductivity, J. Appl. Phys., 2018, 124, 165101.

26 S. J. R. Tan, S. Sarkar, X. X. Zhao, X. Luo, Y. Z. Luo, S. M. Poh, I. Abdelwahab, W. Zhou, T. Venkatesan, W. Chen, S. Y. Quek and K. P. Loh, Temperature- and Phase-Dependent Phonon Renormalization in 1T'-MoS_2, ACS Nano, 2018, 12, 5051–5058.

27 G. Kresse and J. Furthmu¨ller, Efficient Iterative Schemes for Ab Initio Total-Energy Calculations Using a Plane-Wave Basis Set, Phys. Rev. B: Condens. Matter Mater. Phys., 1996, 54, 11169–11186.

28 G. Kresse and J. Furthmu¨ller, Efficiency of Ab-Initio Total Energy Calculations for Metals and Semiconductors Using a Plane-Wave Basis Set, Comput. Mater. Sci., 1996, 6, 15–50.

29 J. Ihm, A. Zunger and M. L. Cohen, Momentum-space formalism for the total energy of solids, J. Phys. C: Solid State Phys., 1979, 12, 4409.

30 P. E. Blo¨chl, Projector Augmented-Wave Method, Phys. Rev. B: Condens. Matter Mater. Phys., 1994, 50, 17953–17979.

31 G. Kresse and D. Joubert, From Ultrasoft Pseudopotentials to the Projector Augmented-Wave Method, Phys. Rev. B: Condens. Matter Mater. Phys., 1999, 59, 1758–1775.

32 N. Lu, H. Y. Guo, L. Li, J. Dai, L. Wang, W. N. Mei, X. J. Wu and X. C. Zeng, MoS_2/MX_2 heterobilayers: bandgap engi-neering via tensile strain or external electrical field, Nano-scale, 2014, 6, 2879–2886.

33 S. Manzeli, D. Ovchinnikov, D. Pasquier, O. V. Yazyev and A. Kis, 2D transition metal dichalcogenides, Nat. Rev. Mater., 2017, 2, 17033.

34 G. Eda, T. Fujita, H. Yamaguchi, D. Voiry, M. W. Chen and M. Chhowalla, Coherent Atomic and Electronic Heterostruc-tures of Single-Layer MoS_2, ACS Nano, 2012, 6, 7311–7317.

35 J. Heising and M. G. Kanatzidis, Structure of Restacked MoS_2 and WS_2 Elucidated by Electron Crystallography, J. Am. Chem. Soc., 1999, 121, 638–643.

36 L. F. Wang, Z. Xu, W. L. Wang and X. D. Bai, Atomic Mechanism of Dynamic Electrochemical Lithiation Pro-cesses of MoS_2 Nanosheets, J. Am. Chem. Soc., 2014, 136, 6693–6697.

37 G. Eda, H. Yamaguchi, D. Voiry, T. Fujita, M. W. Chen, M. W. Chen and M. Chhowalla, Photoluminescence from Chemically Exfoliated MoS_2, Nano Lett., 2011, 11, 5111–5116.

38 A. Syahroni, A. B. Cahaya and M. A. Majidi, Quasiparticle electronic structure of 1T'-MoS_2 within GW approximation, J. Phys.: Conf. Ser., 2019, 1245, 012085.

39 Y. D. Fu, X. X. Feng, M. F. Yan, K. Wang and S. Y. Wang, First principle study on electronic structure and optical phonon properties of 2H-MoS_2, Phys. B, 2013, 426, 103–107.

40 Y. Y. Gan and H. J. Zhao, Chirality eff ect of mechanical and electronic properties of monolayer MoS_2 with vacancies, Phys. Lett. A, 2014, 378, 2910–2914.

41 H. T. Wang, Z. Y. Lu, S. C. Xu, D. S. Kong, J. J. Cha, G. Y. Zheng, P.-C. Hsu, K. Yan, D. Bradshaw, F. B. Prinz and Y. Cui, Electrochemical tuning of vertically aligned MoS_2 nanofilms and its application in improving hydrogen evolution reaction, Proc. Natl. Acad. Sci. U. S. A., 2013, 110, 19701–19706.
42 H. Li, C. Tsai, A. L. Koh, L. L. Cai, A. W. Contryman, A. H. Fragapane, J. H. Zhao, H. S. Han, H. C. Manoharan, F. Abild-Pedersen, J. K. Nørskov and X. L. Zheng, Activating and optimizing MoS_2 basal planes for hydrogen evolution through the formation of strained sulphur vacancies, Nat. Mater., 2016, 15, 48–53.
43 G. P. Gao, Y. Jiao, F. X. Ma, Y. L. Jiao, E. R. Waclawik and A. J. Du, Charge Mediated Semiconducting-to-Metallic Phase Transition in Molybdenum Disulfide Monolayer and Hydrogen Evolution Reaction in New $1T^0$ Phase, J. Phys. Chem. C, 2015, 119, 13124–13128.
44 R. F. W. Bader, A quantum theory of molecular structure and its applications, Chem. Rev., 1991, 91(5), 893–928.